HHS Public Access

Author manuscript

Clin Pharmacol Ther. Author manuscript; available in PMC 2019 February 14.

Published in final edited form as:

Clin Pharmacol Ther. 2016 October ; 100(4): 371–379. doi:10.1002/cpt.367.

Improved Prediction of Drug-Induced Torsades de Pointes Through Simulations of Dynamics and Machine Learning Algorithms

M Cummins Lancaster[1] and **EA Sobie**[1]

[1]Department of Pharmacology and Systems Therapeutics, Icahn School of Medicine at Mount Sinai, New York, New York, USA.

Abstract

The ventricular arrhythmia Torsades de Pointes (TdP) is a common form of drug-induced cardiotoxicity, but prediction of this arrhythmia remains an unresolved issue in drug development. Current assays to evaluate arrhythmia risk are limited by poor specificity and a lack of mechanistic insight. We addressed this important unresolved issue through a novel computational approach that combined simulations of drug effects on dynamics with statistical analysis and machine-learning. Drugs that blocked multiple ion channels were simulated in ventricular myocyte models, and metrics computed from the action potential and intracellular (Ca^{2+}) waveform were used to construct classifiers that distinguished between arrhythmogenic and non-arrhythmogenic drugs. We found that: (1) these classifiers provide superior risk prediction; (2) drug-induced changes to both the action potential and intracellular (Ca^{2+}) influence risk; and (3) cardiac ion channels not typically assessed may significantly affect risk. Our algorithm demonstrates the value of systematic simulations in predicting pharmacological toxicity.

The prediction of drug-induced Torsades de Pointes (TdP) remains a critical issue in drug development. TdP, a rare but potentially fatal ventricular arrhythmia, is a leading cause of drug withdrawal and relabeling. This arrhythmia is caused by a motley range of compounds, including not only cardiovascular drugs, but also antibiotics, antipsychotics, antihistamines, chemotherapeutics, and others. The common molecular mechanism behind the diverse set of TdP-prolonging drugs was identified as a blockade of the KCNH2, or hERG, channel,[1,2] which carries the rapid delayed rectifier K^+ current (I_{Kr}), a key repolarizing current in the human ventricular myocardium. Reduction in I_{Kr} increases the action potential duration (APD), which appears as an increased QT interval on the electrocardiogram. For this reason, current guidelines from the International Conference of Harmonization stipulate that all compounds under development are screened for hERG block and QT prolongation as surrogate markers of TdP risk.[3] The ***in vitro*** hERG block assay is relatively easy to implement, but alone is only a fair predictor of QT[4] and of TdP.[5] Progression to QT studies

---

Correspondence: EA Sobie (eric.sobie@mssm.edu).

AUTHOR CONTRIBUTIONS

E.A.S. and M.C.L. wrote the manuscript. E.A.S. and M.C.L. designed the research. M.C.L. performed the research. E.A.S. and M.C.L. analyzed the data.

CONFLICT OF INTEREST

The authors declared no conflict of interest.

in humans or even in animals represents an enormous investment for perhaps only a marginal increase in predictive power. Thus, the need is twofold for a method that both predicts TdP accurately and can be applied inexpensively early in the development process. To this end, a new paradigm is emerging in which ***in silico*** modeling plays a central role.[6,7]

A major shortcoming of the hERG assay is the failure to account for multichannel drug effects. Indeed, it has been known for years that the arrhythmogenicity of hERG block is mitigated by concurrent block of Na^+ or Ca^{2+} channels.[8,9] Recently, Kramer *et* al.[10] published a predictive model that accounts for L-type Ca^{2+} channel block in addition to hERG block. Their model improved discrimination between torsadogenic and non-torsadogenic drugs over the hERG assay, demonstrating that Ca^{2+} current block is a common mitigating factor in drug torsa-dogenicity. However, the mechanism of the protective effect of multichannel block is unclear. It is unlikely that it is purely due to diminished action potential (AP) prolongation, as *in vivo* studies show that multichannel block can reduce hERG blockinduced TdP without reduction of the QT interval.[8,9,11] An alternative possibility is that the protective effect of multichannel block occurs via changes in ion concentration homeostasis. In this case, other physiological metrics, derived from the AP or from intracellular ionic concentrations, may better predict TdP potential.

The goal of this study was twofold. First, we sought to develop a classifier for improved prediction of drug torsadogenicity. Second, we aimed to apply our classifier to identify key cellular physiological differences between torsadogenic and nontorsadogenic drugs. To accomplish these goals, we took a Quantitative Systems Pharmacology approach that combined modeling of physiological dynamics with statistical analysis and machine-learning. Using mechanistic myocyte models allowed us to simulate multichannel drug effects on cellular physiology. We evaluated the simulation results using an unbiased approach, in which we computed a variety of metrics from both the AP and intracellular Ca^{2+} waveforms. Machine-learning algorithms trained by clinical torsadogenicity data were then used to construct a top-performing classifier. Through this approach we obtained the following important results: (1) our classifier provides excellent prediction of torsadogenic risk, superior, to our knowledge, to existing methods; (2) simulations indicate that drug-induced changes to both the AP and intracellular Ca^{2+} influence TdP risk; and (3) the modeling results reveal which cardiac ion channels may have the greatest impact on TdP risk, and are therefore the most important to assess early in the drug development process.

RESULTS

Human ventricular cell models simulate drug response

To predict the physiological effects of a wide range of drugs, we simulated the application of 86 drugs at effective free therapeutic plasma concentration (EFTPC) in three recent, independently formulated human ventricular myocyte models.[12–14] Drugs altered multiple aspects of APs (Figure 1a) and Ca^{2+} transient waveforms (CaTs; Figure 1b), which we quantified by calculating the 13 metrics shown in the Figure 1 insets. Figure 1c shows how the 86 drugs influenced these metrics, a total of 331 under all conditions. The simulations therefore generate a highdimensional set of pseudo-data.

A novel classification method identifies torsadogenic drugs

The original 331 metrics include a diverse range of measurements from the AP and CaT, measured in multiple ventricular cell models under several conditions. This broad sampling captures informative metrics with minimal bias but also contains many correlated or redundant variables. To reduce the dimensionality of this dataset, we calculated its principal components (PCs), and found that the first three PCs describe 88.2% of the variance (Figure 2a). Furthermore, drug scores in two- and three-PC space show a clear division between torsadogenic and nontorsa-dogenic drugs (Figure 2b,c).

The drug scores in the PC space were used to train a support vector machine (SVM) classifier. This classification algorithm, appropriate for discrimination when samples fall into two categories,[15] defines a decision boundary in the space such that drugs on one side of the decision boundary are predicted to be torsado-genic, and drugs on the other side are predicted to be nontorsadogenic. In building the SVM, we found that including more than three PCs did not improve classifier performance.

The SVM classifier performance was evaluated with several methods. With leave-one-out cross-validation, we found that the SVM correctly classifies 87.2% and misclassifies 12.8% of the drugs studied (Figure 2e and Table 1, “dose-dependent classifier”). Using receiver operating characteristic (ROC) analysis[16] to evaluate classifier performance, we found that the area under the ROC curve (auROC) was 0.963, indicating strong predictive power (auROC = 0.5 and auROC = 1 indicate no predictive power, and perfect prediction, respectively). This performance is a substantial improvement over classifications based on either hERG block or APD at 90% repolarization (APD_{90}), which had auROCs of 0.815 and 0.854, respectively (Figure 2d). The Matthews correlation coefficient and the F1 score (see Methods) also confirmed improved classification compared with these alternative metrics (Supplementary Table S1).

Ca^{2+} dynamics augment action potential duration to identify torsadogenic drugs

Classification based on specific simulated metrics rather than PC scores provides physiological insight into differences between drugs. Because the PC analysis indicates that two to three orthogonal dimensions are sufficient to distinguish torsadogenic from nontorsadogenic drugs, we hypothesized that two to three metrics may allow for accurate drug classification. To test this, we performed feature selection on the 331 metrics, as described in Supplementary Text. We found that two metrics, APD at 50% repolarization (APD_{50}) and diastolic $(Ca^{2+})_i$, both measured at 1 Hz in the O’Hara, Virág, Varró, and Rudy (OVVR) epicardial-model,[14] provide comparable discrimination between torsadogenic and nontorsadogenic drugs, with an auROC = 0.962 in leave-one-out cross-validation (Figure 3a).

As expected, drugs with dramatic AP prolongation are torsadogenic (Figure 3b). More interestingly, drugs with moderate AP prolongation can fall into either category (Figure 3b **inset**). A measurement of Ca^{2+} dynamics, the diastolic $(Ca^{2+})_i$, provides the additional information necessary to classify these drugs. That is, although many torsadogenic and nontorsadogenic drugs may cause the same extent of moderate AP prolongation,

nontorsadogenic drugs consistently result in lower intracellular (Ca^{2+}). For example, dofetilide, a torsadogenic class III antiarrhythmic, and piperacillin, a safe beta-lactam antibiotic, cause nearly identical simulated AP-prolongation. The former drug, however, increases diastolic Ca^{2+} and CaT amplitude, whereas piperacillin has opposite effects (Figure 3c).

Risk prediction is robust across a large range of doses

Our classifier is based on simulations performed with each drug at its typical clinical concentration (EFTPC), a variable that is unlikely to be known early in drug development. To develop a method that does not require EFTPC, we repeated the classification analysis after simulating each drug at 0.1, 1, 10, and 100 times EFTPC. Because the 35 drugs in the highest CredibleMeds risk category (“risk of Torsades”) averaged 2.5 units from the decision boundary at EFTPC, we considered 2 units as our threshold of +TdP prediction. Figure 4 shows the dose dependence of each drug’s distance from the decision boundary. Larger positive/negative distances from the boundary can be interpreted as stronger predictions of torsadogenicity/nontorsadogenicity, respectively.

As drug concentration increases, truly dangerous drugs reveal their risk (Table 1). For instance, amiodarone, imipramine, and solifenacin were close to the origin at EFTPC, but higher concentrations of these drugs moved them onto the correct, torsadogenic side of the decision boundary.

However, several “safe” drugs are predicted to be dangerous at extreme concentrations (100× EFTPC). These drugs were close to the decision boundary at EFTPC, and moved onto the wrong side at the highest concentrations. Interestingly, a drug that we classified as such a false-positive, donepezil, was identified as torsadogenic by CredibleMeds after the completion of this study. Furthermore, four of the remaining false-positives, quetiapine, diphenhydramine, amitriptyline, and fluvoxamine, have case reports of TdP.[5,6,17] Therefore, our classification algorithm correctly predicted the torsadogenicity of donepezil, and it seems to be identifying drugs with the capacity to produce TdP at extremely high doses, albeit with not enough current evidence to meet the criteria for the torsadogenic category.

Importantly, this evaluation over a four-order of magnitude concentration range suggests a procedure for classifying drugs in preclinical development, when EFTPC is not yet known. Each candidate drug would be simulated at increasing concentrations until its score reaches a predetermined distance from the decision boundary, at which point its risk will be predicted. This approach was validated with our trial set of drugs and correctly classified 89.5% of drugs (Table 1, “dose-independent classifier”), with an area under the curve of 0.936 (Supplementary Figure S2).

A synthetic population stratifies drug risk

Differences between individuals in ionic current properties can influence differential drug responses, such as the wide range in AP prolongation seen with hERG-blocking drugs due to variability in repolarization reserve.[18–20] To study the role of interindividual variation in predicting drug arrhythmia risk, we generated a synthetic population of 24 individuals by randomly varying ionic current parameters and calibrating the population variability to

experimental data[21] (see Supplementary Text for details). The full drug set was simulated in each of the 24 individuals, and drug risk was determined using the classifier built on APD_{50} and diastolic Ca^{2+} simulated in the OVVR model.

Simulating drug effects in a synthetic population allows us to compute probabilities of TdP risk, because a given drug may be classified as torsadogenic in some individuals and nontorsadogenic in others. Drugs with a well-established, high risk of Torsades (CredibleMeds risk category 1, red bars) had a positive prediction in several, sometimes even in a majority of individuals (Figure 5a). Drugs with a probable risk of Torsades (Credible-Meds risk category 2, pink bars), tended to have positive predictions in a low but substantial portion of the population (up to 16.7%). Drugs in the "conditional risk" category (CredibleMeds risk category 3, cyan bars) had 0–1 positive predictions. Finally, drugs with no known risk of Torsades (blue bars) were generally predicted to be safe in all individuals, although several had a positive prediction in a single individual. Therefore, evaluation in the synthetic population may provide a prediction of the degree of risk and incidence of Torsades. Figure 5b illustrates this with three example drugs: ibutilide, nitrendipine, and nilotinib. Ibutilide, a class III antiarrhythmic with a well-established risk of Torsades, is predicted to be dangerous in the majority (71%) of individuals. In contrast, nitrendipine is a dihydropyridine Ca^{2+}-channel blocker with no known risk of Torsades that is predicted to be safe in all individuals in the population. Finally, nilotinib, a small-molecule tyrosine kinase inhibitor with a black box warning for QT-prolongation and sudden death,[22] is predicted to be safe in the majority of individuals, but torsadogenic in a subset (12.5%).

To compare this approach to the results presented earlier, Figure 5c shows, for each drug, the percent of the population with a positive risk prediction vs. the drug's distance from the decision boundary in the simulations that did not incorporate variability. For drugs with a positive prediction in at least one individual, we found that this distance has a strong correlation with the proportion of the population in which the drug is predicted to be torsadogenic. Additionally, drugs initially predicted to be nontorsadogenic also had a negative prediction in 96–100% of the population. This demonstrates that the severity of risk is consistently predicted by both the population approach and the distance from the decision boundary.

Off-target interactions influence drug risk

Because our classifier is based on physiological metrics, it can be used to predict the torsadogenicity of any drug that affects the AP and CaT. This means that drug targets other than those in the training set can be evaluated. To predict which additional targets are the most influential, we generated 100 hypothetical drugs that alter the activity of nine ion channels, pumps and transporters distinct from those targeted by the original drug set. These drug actions were simulated by varying the model parameters governing the activity of each target molecule (e.g., ion channel maximal conductance). By simulating the application of these hypothetical drugs, we could apply the SVM classifier and predict which drugs would cause TdP and which would not.

We used this set of hypothetical drugs to predict the influence of each parameter on drug risk. Influence was determined by performing a Wilcoxon rank sum test between the drugs

with positive and negative predictions of TdP (Supplementary Table S2). Figure 6a shows the four targets with the most significant effects on predicted drug risk via a “wheel of fortune”-style plot (as in refs. 23,24). Each radial “slice” represents one drug: how it alters each of the four targets and the resulting risk. We predict that alterations to the Na^+-Ca^{2+} exchanger have the largest effect on TdP risk, with increased current leading to decreased risk. The Na^+-K^+ ATPase, background Ca^{2+} current and the SERCA pump followed in significance (Supplementary Table S2). In other words, this analysis predicts that these four currents have a large influence on Torsades risk, meaning that the torsadogenic risk of some drugs may be modulated by off-target drug interactions with these ion transport pathways.

To investigate the influence of these parameters further, we performed simulations in which each parameter was individually perturbed at intervals from 50–200% of the control value. We found that increases in the activity of the Na^+ -K^+ ATPase and the Na^+ -Ca^{2+} exchanger were protective, whereas decreases were predicted to be torsadogenic (Figure 6b). Note, however, that enhancing the exchanger activity by more than ~400% results in a prediction of Torsades risk (Supplementary Figure S3a). It is likely that moderately increased exchanger activity is favorable due to decreased Ca^{2+} load, but even larger activity levels may cause excessive AP prolongation. This is supported by simulations in which a 10-fold increase in exchanger activity resulted in an EAD in the OVVR model (Supplementary Figure S3b). One caveat of this analysis is that some predictions fall in regions of risk space that do not contain any data from real drugs, so the prediction that these combinations of physiological changes are torsadogenic is not well-supported. This is the case for decreased activity of both the ATPase and the exchanger.

The perturbations to the exchanger and the ATPase are compared to perturbations to the maximal conductance of the slow delayed rectifier (G_{Ks}) and the inward rectifier (G_{K1}) in Figure 6b. As expected, blocking either K^+ current is predicted to be torsadogenic, and enhancing either is protective. Interestingly, and consistent with the hypothetical drug analysis (Supplementary Table S2), the magnitude of the effects of perturbing the K^+ currents is less than that of perturbing the exchanger or pump, supporting the idea that alterations in ion concentration homeostasis may play a central role in torsadogenesis.

DISCUSSION

We have developed a classifier, with superior prediction of torsadogenic risk, for use in early drug development. To do this, we took a Quantitative Systems Pharmacology strategy, running extensive mechanistic simulations based on results from a large drug dataset. This provided advantages over more traditional approaches. First, by comprehensively evaluating multiple parameters, multiple outputs, and a large set of drugs, we were able to abstract general rules that would not have been apparent from focused studies on select drugs. Second, our time course simulations provide deeper insight into the physiological mechanisms of drug action than the “snapshot” one obtains using high throughput measurements, such as ion channel block or altered gene expression. These two aspects, simulations of dynamics and relatively large scale analysis, are essential ingredients in the emerging discipline of Quantitative Systems Pharmacology.

The prediction of drug-induced TdP is an unresolved issue in drug development. Since the institution of the ICH S7B and E14 guidelines for cardiac safety testing in 2005,[3] no new torsadogenic drugs have reached the market. However, it is widely recognized that the TdP surrogates mandated by these guidelines, hERG block and QT prolongation, are nonspecific and most likely prevent the development of efficacious, nontorsadogenic drugs.[7] The use of *in silico* screening methods, such as the classifier described in this study, has the potential both to reduce the rejection of truly safe drugs and to shift attrition of dangerous drugs to earlier stages of development. Our classifier is specifically designed for use in early drug development, as it requires only *in vitro* data that are typically acquired prior to animal or human studies (IC_{50} values for hERG, $Na_v1.5$, and $Ca_v1.2$). In this sense, our approach builds on prior work to design drug classifiers.[6,10] For instance, a predictive model based on changes in APD_{90} after simulated exposure to drug demonstrated the importance of multichannel block.[6] Subsequently, Kramer *et al.*[10] developed a high-performing classification model that did not involve simulations but required only the ratio between hERG and $Ca_v1.2$ blocking potencies. Our classifier, which incorporates multichannel block, simulated physiological responses, multiple myocyte models, and large sets of simulated data, can identify torsadogenic drugs with a misclassification rate of 12.8% and an auROC of 0.963 under leave-one-out cross-validation (Figure 2). This is the highest performing drug-induced TdP predictor that we are aware of.

Our study demonstrates the value of simulations to not only predict cellular drug responses, but to direct experimental studies. Specifically, simulations such as those presented here can: (1) inform drug inhibition experiments by prioritizing which channels to examine (Figure 6); and (2) assist in the design of *in vitro* cellular studies by demonstrating that metrics derived from CaTs are also useful in predicting TdP risk (Figure 3).

A benefit of our strategy is that we do not assume the primacy of particular physiological responses, such as AP prolongation. Instead, we calculate from simulations a wide range of metrics, and then systematically determine which are most informative. In principle, this same approach can be used to evaluate the predictive utility of other proposed surrogates, such as Triangulation, Reverse use dependency, electrical Instability of the action potential, and Dispersion (TRIaD),[25] the electromechanical window,[26] and beat-to-beat variability of repolarization.[27] These particular questions, however, must be addressed with models that simulate additional phenomena, such as stochastic ion channel gating and drug effects on multidimensional tissue. Nonetheless, this study illustrates a general method to determine the most appropriate surrogates for drug-induced adverse events, a strategy that can be extended to predict other types of toxicity.

An important result was the finding that drug-induced changes in diastolic (Ca^{2+}) were nearly as important as changes in APD to differentiate between torsadogenic and nontorsadogenic drugs. Additionally, our simulations with hypothetical drugs identified the Na^+-K^+ ATPase, Na^+-Ca^{2+} exchanger, background Ca^{2+} current, and the SERCA pump as the most significant potential modulators of TdP risk. Taken together, these findings indicate a major role for Ca^{2+} homeostasis in TdP generation. During the prolonged AP plateau caused by QT-prolonging drugs, more Ca^{2+} enters the myocyte with each beat. This alteration to Ca^{2+} homeostasis can have several effects, including higher SR Ca^{2+} load,

activation of Ca^{2+}-calmodulin dependent kinase II, and further membrane depolarization when Ca^{2+} is extruded from the cell via Na^{+}-Ca^{2+} exchange. Indeed, when viewed in light of recent experimental studies indicating that hERG block may lead to spontaneous cellular Ca^{2+} release,[28,29] our simulations suggest a central role of intracellular Ca^{2+} in the generation of TdP.

Because we designed our classification algorithm for use early in drug safety testing, the characteristics of data available at this stage impose several limitations. We use measurements of inhibition of I_{Kr}, I_{CaL}, and I_{Na}, but interaction with additional channels will also influence risk, as our simulations suggest (Figure 6). Moreover, the measurement of peak I_{Na} inhibition does not account for specific effects on the late Na^{+} current (I_{NaL}). Because this current can potentiate the torsadogenicity of hERG-blocking drugs,[30] specific measurements of I_{NaL} block, and improved representations of this current in mathematical models, would likely improve classifier performance. Because early safety testing does not include the detailed measurements needed to parameterize more complex models, we use the simple pore-block model of drug action, which does not account for the kinetics of channel block or state-dependent drug binding. Our method also does not include drug effects on channel trafficking, which plays a role in the torsadogenesis of some drugs.[31,32] Drug safety testing, however, continues to evolve, and routine *in vitro* tests may soon include both block of additional channels and protocols designed to detect effects on channel expression and regulation. Modification of our classifier to include these additional measurements would be straightforward and may improve its predictive ability. Nevertheless, even with simple inputs, our classifier identifies clinically torsadogenic drugs with high accuracy.

METHODS

Complete methods are provided in the online Supplementary Information, with only a few critical aspects of the procedures highlighted here.

Models and simulations

Each drug was simulated in three human ventricular myocyte models. To avoid any potential bias resulting from the model development choices of a particular research group, we conducted simulations in three independent models: (1) OVVR[14]; (2) ten Tusscher and Panfilov[12]; and (3) Grandi, Pasqualini, and Bers.[13] Drug effects on three important ion channels were simulated with a simple pore block model described in the Supplementary Information. Simulated myocytes were electrically stimulated at rates of 2 Hz, 1 Hz, and 0.5 Hz to steady state.[33] In total, each drug was simulated under 24 different conditions: at 3 pacing rates × 8 cell types (3 transmural layers in OVVR and ten Tusscher and Panfilov, 2 layers in Grandi, Pasqualini, and Bers). For each drug under each of the 24 conditions, we calculated several metrics from the APs and intracellular (Ca^{2+}) time courses (Figure 1, Supplementary Table S3).

Initial simulations examined each drug at its EFTPC and simulated each model with its baseline, published parameters. Later simulations examined: (1) multiple concentrations of each drug; (2) a population of cells exhibiting biological variability[19,34,35]; and (3)

hypothetical drugs that inhibited additional ion transport pathways, as described in the Supplementary Information.

Databases

Drug inhibition of the rapid delayed rectifier K^+ current (I_{Kr}), the L-type Ca^{2+} current (I_{CaL}), and the fast Na^+ current (I_{Na}) was incorporated into our classification algorithm using reported half-maximal inhibitory concentrations (IC50). We obtained these data for 86 drugs published in the studies by Kramer *et al.*[10]and Mirams *et al.*[6] which constitute our drug training set (Supplementary Table S4).

We defined the torsadogenicity of the drugs in our training set using the CredibleMeds database (https://www.crediblemeds.org) and the study from Champeroux *et al.*[36] as described in the Supplementary Text.

Classification of drugs

To reduce the dimensionality of the dataset containing 331 metrics, the PCs of the metrics were calculated. These PCs were used to train a SVM classifier[15] with a linear kernel. The SVM classifier defined a planar decision boundary in the PC space using the sequential minimal optimization algorithm, with a box constraint of one, to determine the boundary with a maximal margin between the two categories. Classification was performed with leave-one-out cross validation (i.e., the SVM used to predict any particular drug was built using only results from the remaining drugs in the dataset). Classifier performance was evaluated through three methods: (1) calculating an ROC curve; (2) the Matthews correlation coefficient, based on true and false-positives and true and false-negatives[16]; and (3) the F1 score, based on sensitivity and positive predictive value.[37]

Supplementary Material

Refer to Web version on PubMed Central for supplementary material.

ACKNOWLEDGMENTS

Research in Dr. Sobie's laboratory is supported by the National Heart, Lung, and Blood Institute (R21 HL122564), the National Institute of General Medical Sciences (P50 GM071558), and the National Institutes of Health Common Fund (U54 HG008098). Dr. Lancaster has been supported by training grants from the National Institute of General Medical Sciences (T32 GM062754 and T32 GM007280).

References

1. Mitcheson JS, Chen J, Lin M, Culberson C & Sanguinetti MC A structural basis for drug-induced long QT syndrome. Proc. Natl. Acad. Sci. USA 97, 12329–12333 (2000). [PubMed: 11005845]
2. Sanguinetti MC, Jiang C, Curran ME & Keating MT A mechanistic link between an inherited and an acquired cardiac arrhythmia: HERG encodes the IKr potassium channel. Cell 81, 299–307 (1995). [PubMed: 7736582]
3. Food and Drug Administration, HHS. International Conference on Harmonisation; guidance on S7B nonclinical evaluation of the potential for delayed ventricular repolarization (QT interval prolongation) by human pharmaceuticals; availability. Notice. Fed. Regist. 70, 61133–61134 (2005). [PubMed: 16237859]

4. Gintant G An evaluation of hERG current assay performance: translating preclinical safety studies to clinical QT prolongation. Pharmacol. Ther. 129, 109–119 (2011). [PubMed: 20807552]
5. Redfern WS et al. Relationships between preclinical cardiac electrophysiology, clinical QT interval prolongation and torsade de pointes for a broad range of drugs: evidence for a provisional safety margin in drug development. Cardiovasc. Res. 58, 32–45 (2003). [PubMed: 12667944]
6. Mirams GR et al. Simulation of multiple ion channel block provides improved early prediction of compounds' clinical torsadogenic risk. Cardiovasc. Res. 91, 53–61 (2011). [PubMed: 21300721]
7. Sager PT, Gintant G, Turner JR, Pettit S & Stockbridge N Rechanneling the cardiac proarrhythmia safety paradigm: a meeting report from the Cardiac Safety Research Consortium. Am. Heart J. 167, 292–300 (2014). [PubMed: 24576511]
8. Antoons G et al. Late Na1 current inhibition by ranolazine reduces Torsades de Pointes in the chronic atrioventricular block dog model. J. Am. Coll. Cardiol. 55, 801–809 (2010). [PubMed: 20170820]
9. Johnson DM, de Jong MM, Crijns HJ, Carlsson LG & Volders PG Reduced ventricular proarrhythmic potential of the novel combined ion-channel blocker AZD1305 versus dofetilide in dogs with remodeled hearts. Circ. Arrhythm. Electrophysiol. 5, 201–209 (2012). [PubMed: 22080293]
10. Kramer J et al. MICE models: superior to the HERG model in predicting Torsade de Pointes. Sci. Rep. 3, 2100 (2013). [PubMed: 23812503]
11. Carlsson L, Drews L, Duker G & Schiller-Linhardt G Attenuation of proarrhythmias related to delayed repolarization by low-dose lidocaine in the anesthetized rabbit. J. Pharmacol. Exp. Ther. 267, 1076–1080 (1993). [PubMed: 8263767]
12. Ten Tusscher KH & Panfilov AV Cell model for efficient simulation of wave propagation in human ventricular tissue under normal and pathological conditions. Phys. Med Biol. 51, 6141–6156 (2006). [PubMed: 17110776]
13. Grandi E, Pasqualini FS & Bers DM A novel computational model of the human ventricular action potential and Ca transient. J. Mol. Cell Cardiol. 48, 112–121 (2010). [PubMed: 19835882]
14. O'Hara T, Virág L, Varró A & Rudy Y Simulation of the undiseased human cardiac ventricular action potential: model formulation and experimental validation. PLoS Comput. Biol. 7, e1002061 (2011). [PubMed: 21637795]
15. Ben-Hur A, Ong CS, Sonnenburg S, SchÖlkopf B & Rätsch G Support vector machines and kernels for computational biology. PLoS Comput. Biol. 4, e1000173 (2008). [PubMed: 18974822]
16. Baldi P, Brunak S, Chauvin Y, Andersen CA & Nielsen H Assessing the accuracy of prediction algorithms for classification: an overview. Bioinformatics 16, 412–424 (2000). [PubMed: 10871264]
17. Hasnain M et al. Quetiapine, QTc interval prolongation, and torsade de pointes: a review of case reports. Ther. Adv. Psychopharmacol. 4, 130–138 (2014). [PubMed: 25057346]
18. Britton OJ et al. Experimentally calibrated population of models predicts and explains intersubject variability in cardiac cellular electrophysiology. Proc. Natl. Acad. Sci. USA 110, E2098–E2105 (2013). [PubMed: 23690584]
19. Sarkar AX & Sobie EA Quantification of repolarization reserve to understand interpatient variability in the response to proarrhythmic drugs: a computational analysis. Heart Rhythm 8,1749–1755 (2011). [PubMed: 21699863]
20. Weeke P et al. Exome sequencing implicates an increased burden of rare potassium channel variants in the risk of drug-induced long QT interval syndrome. J. Am. Coll. Cardiol. 63, 1430–1437 (2014). [PubMed: 24561134]
21. Sánchez C et al. Inter-subject variability in human atrial action potential in sinus rhythm versus chronic atrial fibrillation. PLoS One 9, e105897 (2014). [PubMed: 25157495]
22. Shah RR, Morganroth J & Shah DR Cardiovascular safety of tyrosine kinase inhibitors: with a special focus on cardiac repolarisation (QT interval). DrugSaf. 36, 295–316 (2013).
23. Mann SA et al. Epistatic effects of potassium channel variation on cardiac repolarization and atrial fibrillation risk. J Am. Coll. Cardiol. 59,1017–1025 (2012). [PubMed: 22402074]

24. Sadrieh A et al. Quantifying the origins of population variability in cardiac electrical activity through sensitivity analysis of the electrocardiogram. J. Physiol. 591, 4207–4222 (2013). [PubMed: 23551947]
25. Shah RR & Hondeghem LM Refining detection of drug-induced proarrhythmia: QT interval and TRIaD. Heart Rhythm 2, 758–772 (2005). [PubMed: 15992736]
26. Guns PJ, Johnson DM, Van Op den Bosch J, Weltens E & Lissens J The electro-mechanical window in anaesthetized guinea pigs: a new marker in screening for Torsade de Pointes risk. Br. J. Pharmacol. 166, 689–701 (2012). [PubMed: 22122450]
27. Thomsen MB et al. Increased short-term variability of repolarization predicts d-sotalol-induced torsades de pointes in dogs. Circulation 110, 2453–2459 (2004). [PubMed: 15477402]
28. Terentyev D et al. Hyperphosphorylation of RyRs underlies triggered activity in transgenic rabbit model of LQT2 syndrome. Circ. Res. 115, 919–928 (2014). [PubMed: 25249569]
29. Kim JJ, Němec J, Li Q & Salama G Synchronous systolic subcellular Ca2+-elevations underlie ventricular arrhythmia in drug-induced long QT type 2. Circ. Arrhythm. Electrophysiol. 8, 703–712 (2015). [PubMed: 25722252]
30. Wu L, Shryock JC, Song Y & Belardinelli L An increase in late sodium current potentiates the proarrhythmic activities of low-risk QT-prolonging drugs in female rabbit hearts. J. Pharmacol. Exp. Ther. 316, 718–726 (2006). [PubMed: 16234410]
31. Kuryshev YA et al. Pentamidine-induced long QT syndrome and block of hERG trafficking. J. Pharmacol. Exp. Ther. 312, 316–323 (2005). [PubMed: 15340016]
32. Yang T et al. Screening for acute IKr block is insufficient to detect torsades de pointes liability: role of late sodium current. Circulation 130, 224–234 (2014). [PubMed: 24895457]
33. Livshitz L & Rudy Y Uniqueness and stability of action potential models during rest, pacing, and conduction using problem-solving environment. Biophys. J. 97,1265–1276 (2009). [PubMed: 19720014]
34. Cummins MA, Dalal PJ, Bugana M, Severi S & Sobie EA Comprehensive analyses of ventricular myocyte models identify targets exhibiting favorable rate dependence. PLoS Comput. Biol. 10, e1003543 (2014). [PubMed: 24675446]
35. Sobie EA Parameter sensitivity analysis in electrophysiological models using multivariable regression. Biophys. J. 96,1264–1274 (2009). [PubMed: 19217846]
36. Champeroux P et al. Prediction of the risk of Torsade de Pointes using the model of isolated canine Purkinje fibres. Br. J. Pharmacol. 144, 376–385 (2005). [PubMed: 15655517]
37. Powers DMW Evaluation: from precision, recall and F-measure to ROC, informedness, markedness & correlation. J. Mach. Learn. Tech.2,37–63 (2011).

Study Highlights

WHAT IS THE CURRENT KNOWLEDGE ON THE TOPIC?

☑ All potential drugs are screened for TdP arrhythmia liability during development. However, current assays that measure block of the hERG potassium channel and lengthening of the cardiac action potential are limited by poor specificity.

WHAT QUESTION DID THIS STUDY ADDRESS?

☑ Can computational myocyte models that predict changes to both the action potential and intracellular Ca^{2+} provide more accurate Torsades risk prediction?

WHAT THIS STUDY ADDS TO OUR KNOWLEDGE

☑ Arrhythmia risk depends on drug-induced changes to both the action potential and intracellular Ca^{2+}. These changes can be predicted with high accuracy using *in vitro* measurements and computational models suitable for use in early drug development.

HOW THIS MIGHT CHANGE CLINICAL PHARMACOLOGY AND THERAPEUTICS

☑ This method can increase the sensitivity and specificity of TdP arrhythmia screening during drug development.

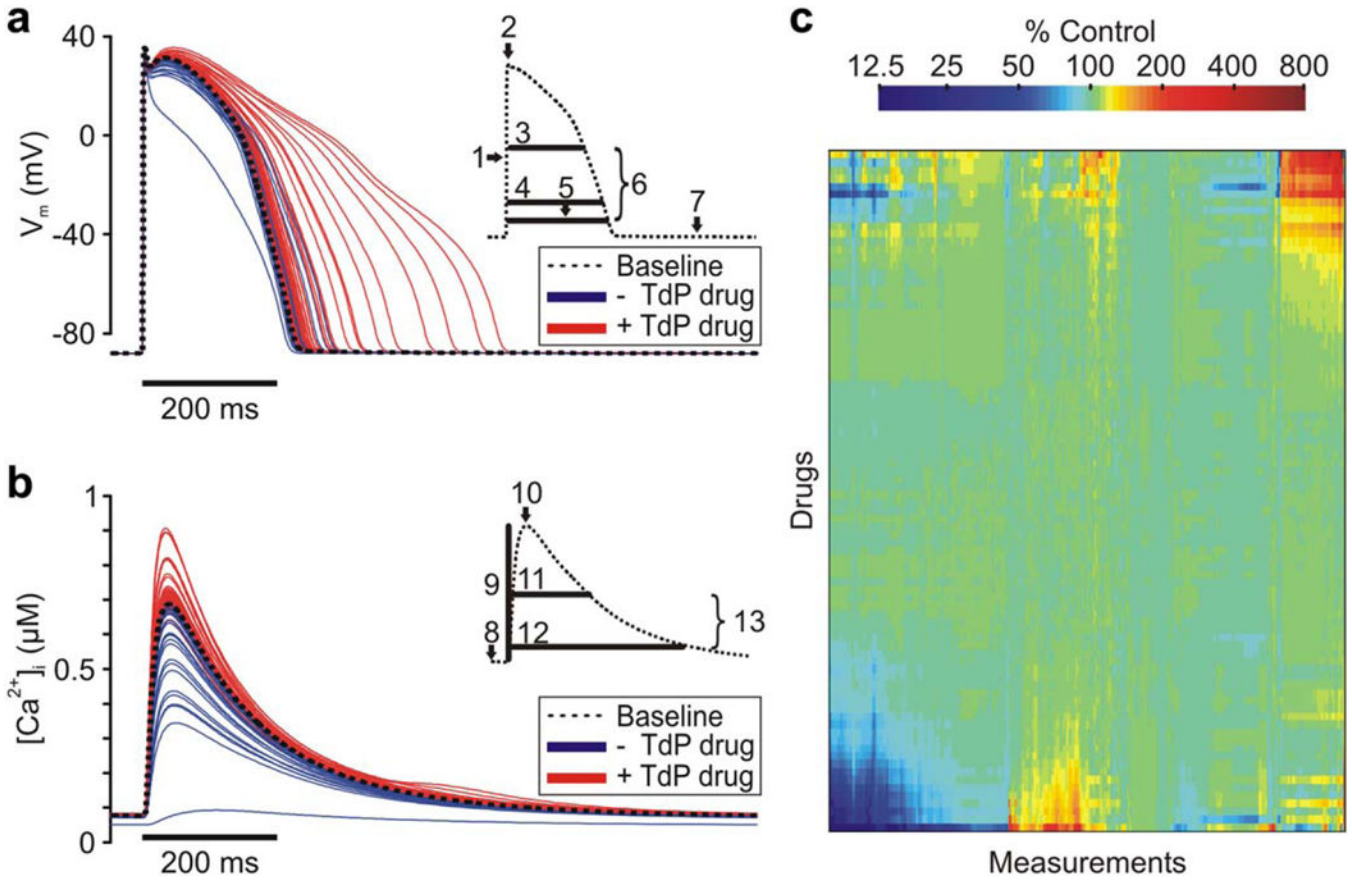

Figure 1.

Drug response in human ventricular cell models. (**a**) Action potential (AP) traces for baseline model and under simulated exposure to each drug. Torsadogenic (+Torsades de Pointes (TdP)) drug APs are red, and nontorsadogenic (-TdP) drug APs are in blue. Inset, AP metrics: (1) upstroke velocity; (2) peak membrane voltage (V_m); (3) AP duration (APD) at 50% repolarization; (4) APD at-60 mV; (5) APD at 90% repolarization; (6) AP triangulation; and (7) resting V_m. (**b**) Ca^{2+} transient (CaT) traces for baseline model and under simulated exposure to each drug. Torsadogenic (+TdP) drug CaTs are red, and nontorsadogenic (-TdP) drug CaTs are in blue. Inset, CaT metrics: (8) resting $(Ca^{2+})_i$ (9) CaT amplitude, (10) Peak $(Ca^{2+})_i$ (11) CaT duration at 50% return to baseline, (12) CaT duration at 90% return to baseline, and (13) CaT triangulation. (**c**) Heatmap of 331 metrics measured under exposure to drug set. Color indicates percent change in metric from baseline value. Drugs and metrics are ordered by unsupervised hierarchical clustering. [Color figure can be viewed in the online issue, which is available at wileyonlinelibrary.com.]

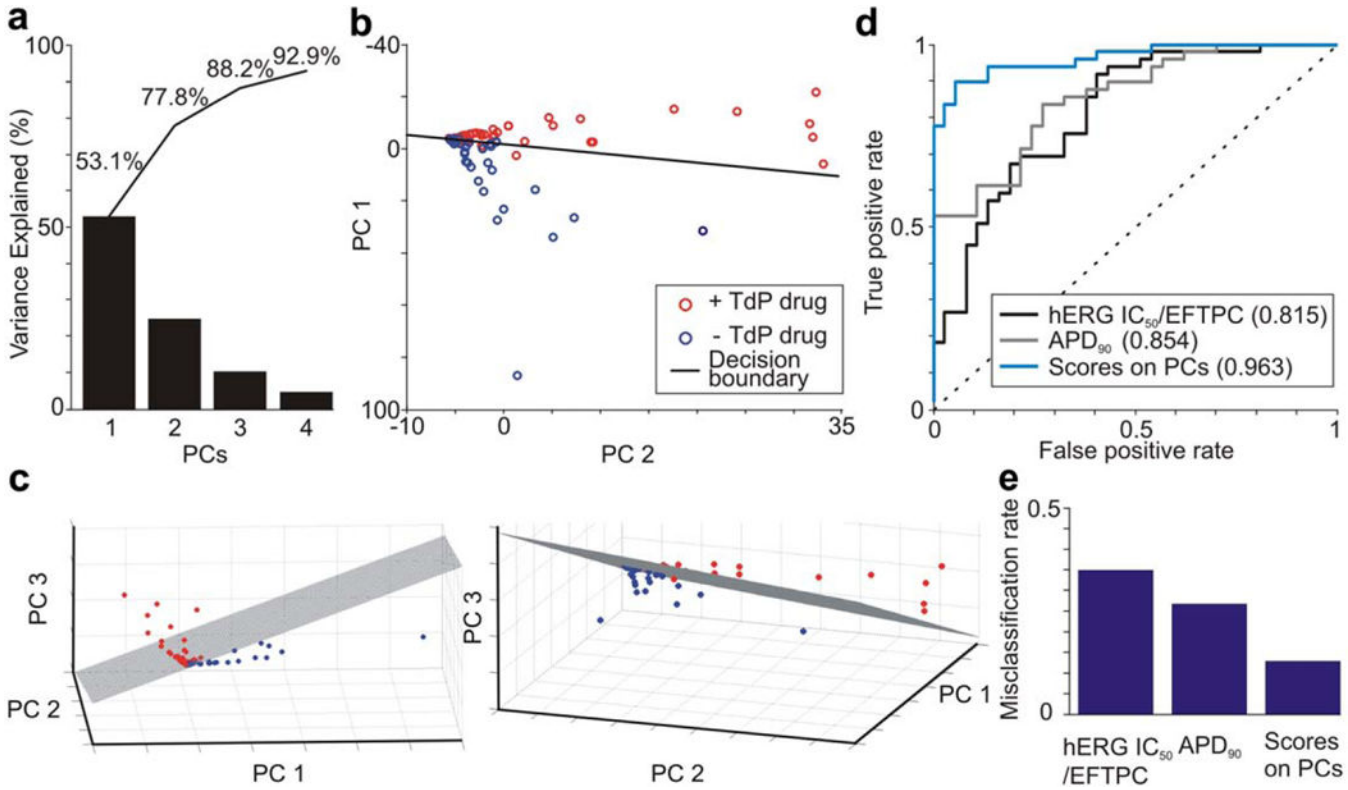

Figure 2.

Principal components (PCs) analysis with support vector machine (SVM) classification discriminates torsadogenic from nontorsadogenic drugs. (**a**) Variance explained by the first four PCs. Cumulative percentages are labeled. (**b**) Drug scores on the first two PCs. SVM decision boundary is shown as a black line, torsadogenic (+Torsades de Pointes (TdP)) drugs are shown as red circles, and nontorsadogenic (-TdP) drugs are shown as blue circles. (**c**) Drug scores on the first three PCs at two viewing angles. SVM decision boundary shown as hatched plane. (**d**) Accuracy of classification assessed using receiver operating characteristic analysis. The SVM model based on drug scores on three PCs is compared to SVM models based on hERG block (hERG IC_{50}/effective free therapeutic plasma concentration (EFTPC)) and action potential duration at 90% repolarization (APD_{90}). Predictive power is quantified by the area under the curve in parentheses in the legend. (**e**) Misclassification rate under leave-one-out cross-validation. [Color figure can be viewed in the online issue, which is available at wileyonlinelibrary.com.]

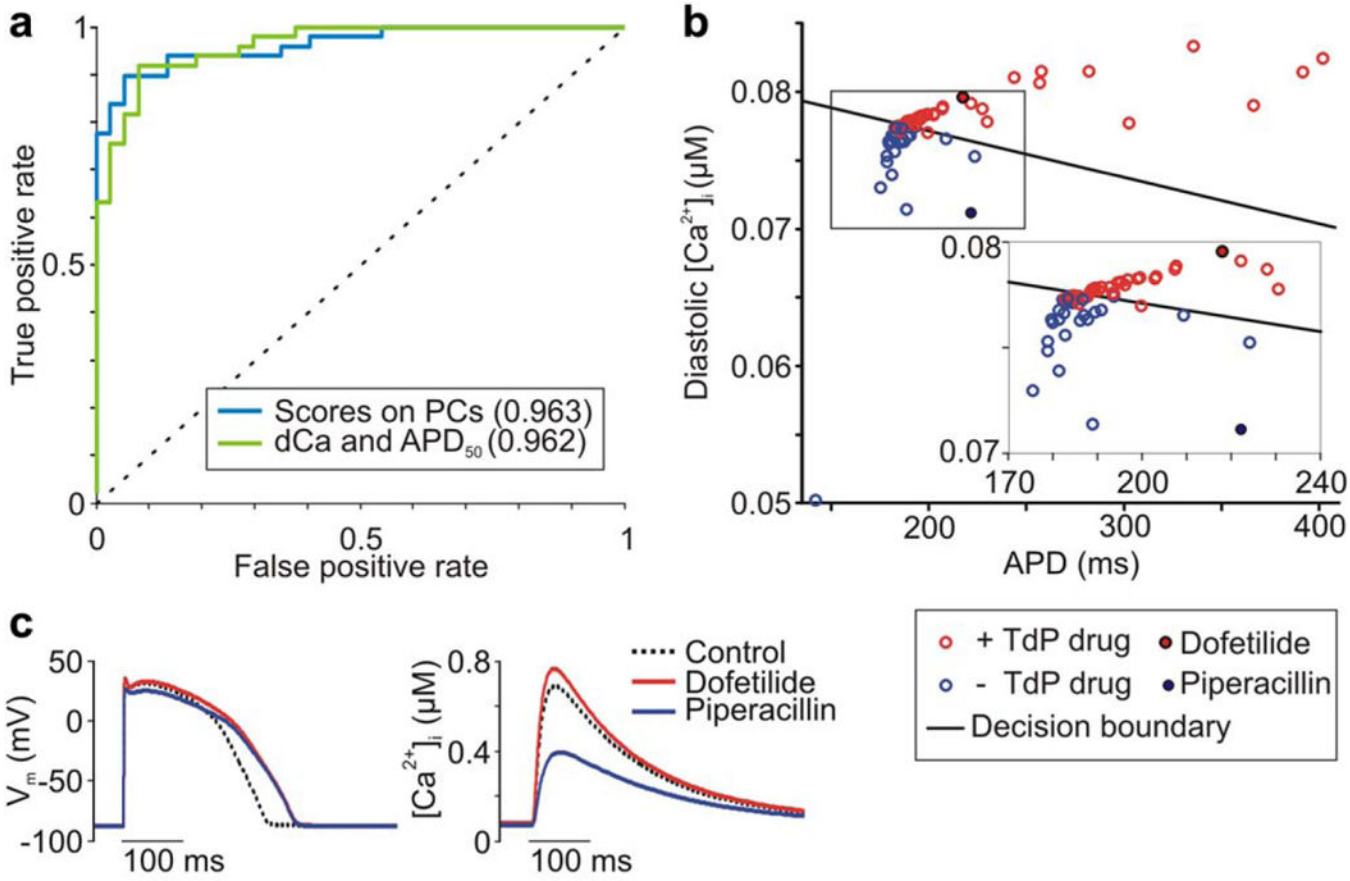

Figure 3.

Selected action potential and Ca^{2+} transient metrics discriminate torsadogenic from nontorsadogenic drugs. (**a**) Accuracy of classification assessed using receiver operating characteristic analysis. The support vector machine (SVM) model based on diastolic Ca^{2+} (dCa) and action potential duration (APD) is compared to the SVM model based on drugs scores on three principal components (PCs). Predictive power is quantified by the area under the curve, listed in parentheses in the legend. (**b**) Diastolic Ca^{2+} (uM) vs. APD (ms) for drug set. SVM decision boundary is shown as a black line, torsadogenic (+Torsades de Pointes (TdP)) drugs are shown as red circles, and nontorsadogenic (-TdP) drugs are shown as blue circles. (**c**) Ca^{2+} transients (right), but not action potentials (left), distinguish dofetilide from piperacillin. [Color figure can be viewed in the online issue, which is available at wileyonlinelibrary.com.]

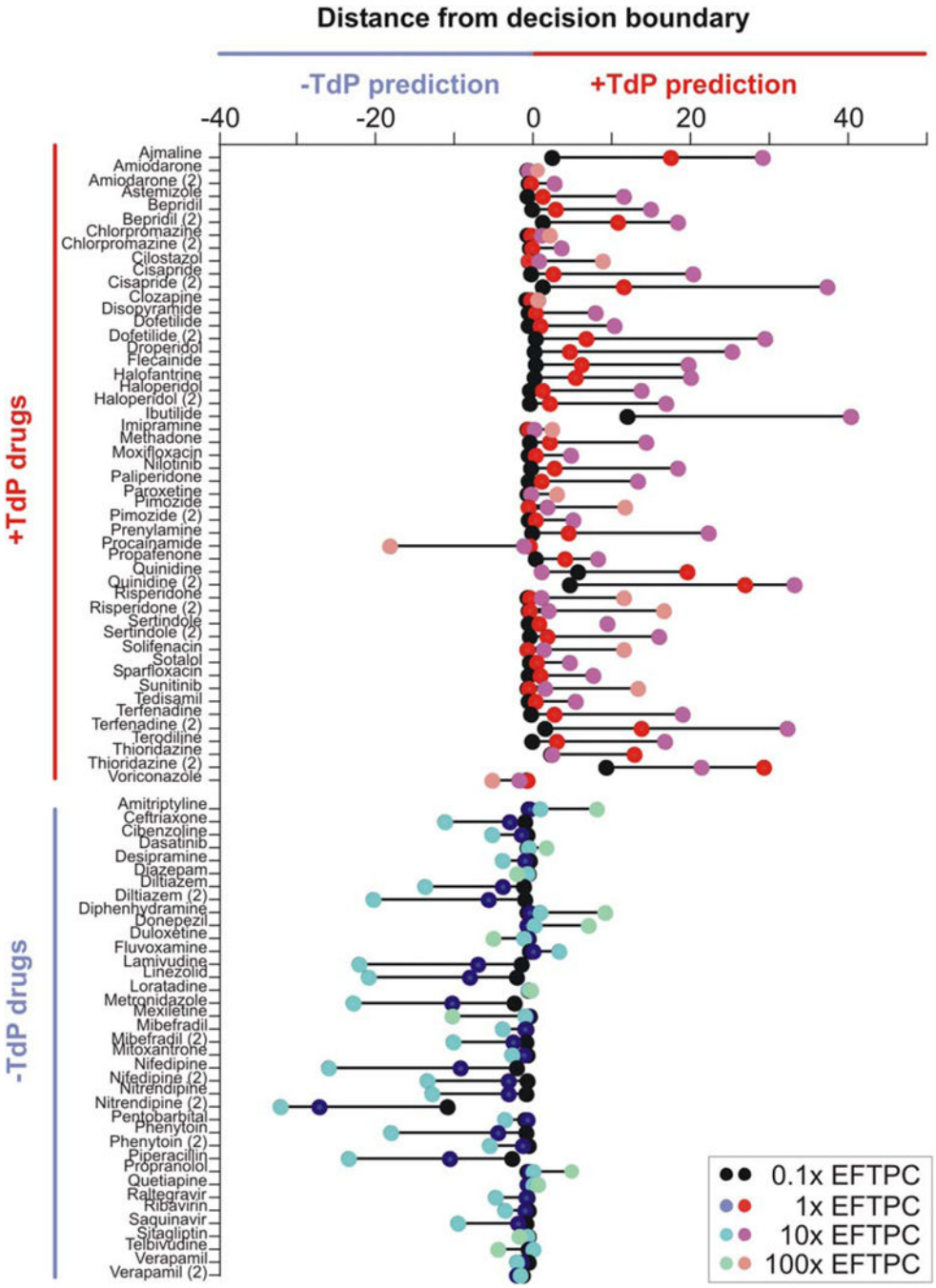

Figure 4.

Dose-dependence of torsadogenicity predictions. Drug distance from decision boundary at concentrations of 0.1,1, 10, and 100 times effective free therapeutic plasma concentration (EFTPC). Positive distance results in a torsadogenic (+Torsades de Pointes (TdP)) prediction, and negative distance results in a nontorsadogenic (-TdP) prediction. Drugs are sorted on the y-axis into known torsadogenic and known nontorsadogenic compounds. [Color figure can be viewed in the online issue, which is available at wileyonlinelibrary.com.]

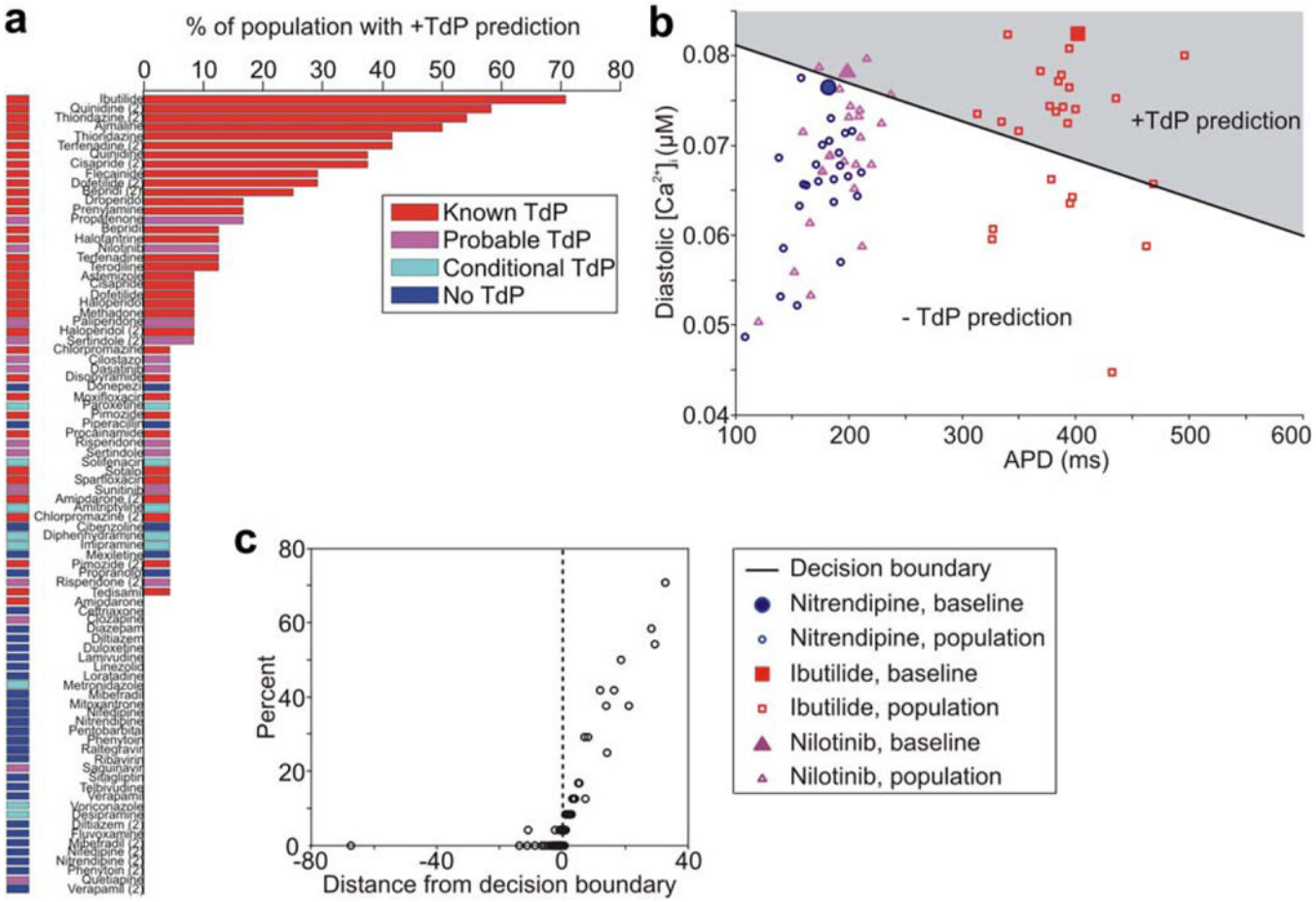

Figure 5.

Drug risk prediction in a synthetic population. (**a**) Percent of individuals in synthetic population in whom each drug is classified as torsadogenic (+Torsades de Pointes (TdP)). Drug bars are colored by known drug risk. (**b**) Population distribution in risk space for ibutilide, nilotinib, and nitrendipine. APD is the action potential duration. (**c**) Percent of population in whom the drug is classified as torsadogenic vs. drug distance from classifier decision boundary in baseline model. Positive distance results in a torsadogenic prediction, and negative distance results in a nontorsadogenic prediction. [Color figure can be viewed in the online issue, which is available at wileyonlinelibrary.com.]

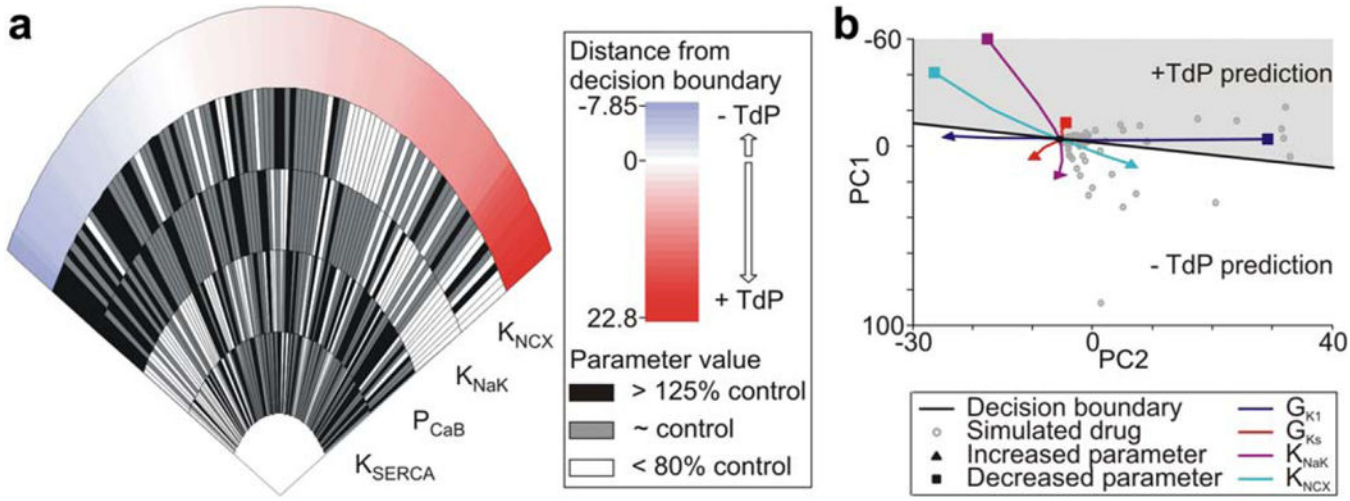

Figure 6.

Most important drug targets in hypothetical drug set. (**a**) The “wheel of fortune” plot shows the four targets with the largest effect on drug risk. Each “slice” represents one drug: how it alters the activity of each of the four targets and the resulting risk. Slices are sorted from left to right by lowest (-Torsades de Pointes (TdP)) to highest (+TdP) predicted risk. Targets are ranked by statistical significance (K_{NCX} p = 1.22E-5, K_{NaK} p = 1.49E-5, P_{CaB} p = 0.000755, and K_{SERCA} p = 0.0312). K_{NCX} is the maximal Na^+-Ca^{2+} exchange current, K_{NaK} scales the Na^+-K^+ ATPase current, P_{CaB} is the background Ca^{2+} current permeability, and K_{SERCA} scales total Ca^{2+} uptake via SERCA pump from myoplasm to NSR. (**b**) Movement in principal component (PC) risk space with single-target perturbations from 50–200% of control values. G_{K1} is the maximal inward rectifier K^+ conductance and G_{Ks} is the maximal slow delayed rectifier K^+ conductance. [Color figure can be viewed in the online issue, which is available at wileyonlinelibrary.com.]

Table 1

Classifier contingency tables and misclassified drugs

	+TdP	−TdP
Dose-dependent classifier		
Correctly classified	46	29
Incorrectly classified	3[a]	8[b]
Dose-independent classifier		
Correctly classified	47	30
Incorrectly classified	2[c]	7[d]

TdP, Torsades de Pointes.

[a] False-negatives in the dose-dependent model were procainamide, voriconazole, and imipramine.

[b] False-positives in the dose-dependent model were amitriptyline, dasatinib, diphenhydramine, duloxetine, fluvoxamine, loratadine, and propranolol.

[c] False-negatives in the dose-independent model were procainamide and voriconazole.

[d] False-positives in the dose-independent model were amitriptyline, dasatinib, diphenhydramine, donepezil, propranolol, fluvoxamine, and quetiapine.